

Hexagonal Sigma–Delta Modulation

Glen Luckjiff and Ian Dobson, *Senior Member, IEEE*

Abstract—A novel application and generalization of sigma–delta ($\Sigma\Delta$) modulation has emerged in three-phase power-electronic converters. A conventional $\Sigma\Delta$ modulator with scalar signals and binary quantizer is generalized to a $\Sigma\Delta$ modulator with vector signals and a hexagonal quantizer. Indeed, power-electronic switching states may be thought of as determining the quantizer outputs. The output spectrum is a key performance measure for both communications and power electronics. This paper analytically derives the output spectrum of the hexagonal $\Sigma\Delta$ modulator with a constant input using ergodic theory and Fourier series on the hexagon. The switching rate of the modulator is important for power-electronic design and formulas for the average switching rate are derived for constant and slowly varying sinusoidal inputs.

Index Terms—Ergodic, power electronics, quantization, sigma–delta ($\Sigma\Delta$) modulation, spectral analysis.

I. INTRODUCTION

THIS PAPER generalizes and applies work in sigma–delta ($\Sigma\Delta$) modulation from the field of communications to a problem of practical significance in power electronics. The system of $\Sigma\Delta$ modulation originated in the sixties and has received significant attention over the past decade as an attractive alternative to conventional analog-to-digital converters [1], [2].

$\Sigma\Delta$ modulators or, more generally, oversampled analog-to-digital converters achieve the performance of high-resolution quantizers by using low resolution quantizers in a feedback loop with linear filtering. These converters modulate an analog signal into a simple code, usually a single bit, at a frequency much higher than the Nyquist rate. In this manner, the modulator can trade resolution in time for resolution in amplitude, as well as employ simple and relatively high-tolerance analog components [2]–[4].

In power electronics, switching converters can also be viewed as analog-to-digital converters wherein an analog reference is coded into a low-resolution set of discrete switching states [5]. Moreover, switching converters typically switch at frequencies well in excess of the Nyquist rate. Therefore, $\Sigma\Delta$ modulation techniques are pertinent. Indeed, $\Sigma\Delta$ modulators have been applied successfully to systems such as resonant link converters wherein the discrete timing of the circuit switching precludes the use of conventional modulation techniques such as pulsewidth modulation (PWM) [5], [6]. Resonant link converters use zero-voltage switching to limit switching losses and attain relatively high switching frequencies [7].

Manuscript received August 30, 2002; revised April 14, 2003. This work was supported in part by the National Science Foundation under Grant ECS-9157192 and Grant ECS-9988574. This paper was recommended by Guest Editor M. di Bernardo.

The authors are with the Electrical and Computer Engineering Department, University of Wisconsin, Madison, WI 53706 USA (e-mail: dobson@engr.wisc.edu).

Digital Object Identifier 10.1109/TCSI.2003.815190

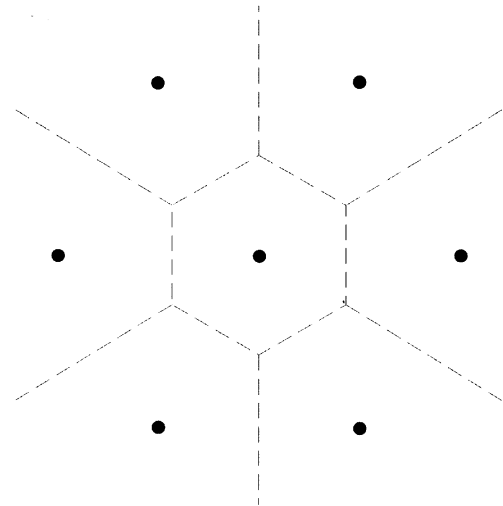


Fig. 1. Output states of voltage-source inverter.

The main analogy we exploit is with the methods in communications theory of converting (modulating) an analog signal to a digital signal with a quantizer and subsequently (after transmission) converting (demodulating) the digital signal back to analog form. For instance, a voltage source converter applies one of a finite set of discrete voltages on the converter output. The converter output is then passed through an analog low-pass filter that removes the modulation frequencies thereby demodulating the discrete voltages back to analog form. In both communications and power electronics, an aim is to design the system so that the input signal is transmitted with minimal distortion.

One consequence of this interpretation is that the power-electronic switching states determine the possible “digitized states” or quantizer outputs. For example, the conventional voltage source inverter [8] has seven switching states which correspond to the seven output vectors in Fig. 1. We assume balanced three-phase signals represented by vectors with three coordinates which sum to zero. The outputs of the voltage-source inverter are the line-to-neutral voltages, which may equal one of seven possible values according to the switch state. These seven space vectors are shown as dots in Fig. 1 and can be thought of as the possible output vectors of a quantizer. Here, we choose the quantizer so that a quantizer input vector u maps to the dot nearest to u . The broken lines in Fig. 1 delimit the regions which map to each dot. This “hexagonal” vector quantizer is a nearest neighbor quantizer and is well known in communications [9], [10]. Moreover, this quantizer is optimal in the sense that the mean-square error from input to output is minimized [9].

To apply the conventional $\Sigma\Delta$ architecture with binary quantization to three-phase converters requires some generalization. First, the output voltages of the voltage source inverter are limited to a set of seven output vectors which form a truncated

hexagonal lattice. If we assume a nearest neighbor partition as in the binary case, the appropriate generalization is the truncated hexagonal vector quantizer discussed above. Second, all modulator signals are augmented from scalar quantities to vectors and a vector integrator replaces the scalar integrator.

There has been extensive design and analysis of scalar $\Sigma\Delta$ modulators for applications in communications and signal processing [1]. Also, vector quantization is applied (but not to $\Sigma\Delta$ modulation) in a number of applications in signal processing [11]. The power-electronic application combines specific vector quantizers with $\Sigma\Delta$ modulation and requires a significant generalization of the scalar work. The vector generalization motivated by the power-electronic application is natural enough in communications and signal processing since the nearest neighbor quantizer is one of the simplest vector quantizers. However, it appears that the use of hexagonal quantizers in $\Sigma\Delta$ modulators has been largely neglected.

Two different approaches for analyzing $\Sigma\Delta$ modulators have evolved: approximate methods based on the results of Bennett [12] and exact analysis. In the first approach, one tries to approximate the quantization noise by choosing an input-independent additive noise source having a similar long-term sample distribution and power spectrum. The simplest noise model is white noise with a uniform distribution. Under such an approximation, the nonlinear $\Sigma\Delta$ modulator is modeled as a linear system, and the performance can readily be derived by using well-known linear system techniques. Moreover, approximate methods have been a key tool in practical design and have predicted many aspects of system behavior to a sufficient degree. Some of the properties agree reasonably well with simulation results [4], [13]. However, two notable failures of the linear model predictions are the generation of idle channel tones and modulator instability [2].

Exact analysis was first applied successfully to discrete-time single-loop $\Sigma\Delta$ modulators with dc input [14], [15]. Instead of assuming the memoryless and uniformity characteristics, this approach derives the true quantizer noise behavior by solving a system of nonlinear difference equations, and then determining the noise statistics and power spectrum. The major conclusion is that the quantizer noise, even though uniformly distributed, is not white. In fact, the quantizer noise and output of single-loop $\Sigma\Delta$ modulators have discrete power spectra, which consists of spectral spikes whose frequency location depend in a complex way on system input [16].

Several researchers have applied exact analysis methods to scalar $\Sigma\Delta$ modulators to describe their behavior, predict their performance, and help develop improved systems. These works share the common goal of avoiding unjustified application of the white noise approximation. Powerful techniques from ergodic theory have been deployed by Gray [14], [16], Delchamps [17], [18], and He *et al.* [19] to derive exact formulas for the spectra of scalar modulators for various inputs. Of related interest are the works of Kieffer [20] on stability and convergence of one-bit quantizers, the work of Hein and Zakhor [21], and the nonlinear dynamics approaches of Wang [22] and Feely [23].

In this paper, we build on these exact analyses to derive the spectrum of a vector $\Sigma\Delta$ modulator with a hexagonal quantizer and a constant input. To simplify our analysis of this highly non-

linear system, we make two assumptions. The first assumption is that the modulator input is constant. While sinusoidal waveforms are also commonly used to test the system performance, the constant input is a useful idealization of slowly varying waveforms. The second assumption is that there is no-overload in the internal quantizer. This can be accomplished by limiting the magnitude of the modulator input (i.e., dynamic range).

A key aspect of modulator performance is the output spectrum. Despite its complexity, we show in this paper that exact calculation of the output spectrum can be done using results from ergodic theory and Fourier analysis. In this approach, the nonlinear discrete dynamical system representing the modulator is thought of as iterated shifts on a torus and the typical statistics of the process may be computed by integration over the torus or subsets of the torus. The generic case of the spectrum calculation first appeared in our conference paper [24].

Switching rate is an important performance measure in power-electronic design since device switching loss is directly proportional to the switching rate. We derive the average switching rate for the scalar and hexagonal $\Sigma\Delta$ modulators with generic constant inputs and then extend this calculation to slowly varying sinusoidal inputs.

There is considerable advantage in using analytic formulas for the output spectrum and switching rate in design because simulation of data with complicated nonperiodic structures has difficulties of run time, data processing, and limited insight into the nature of the process and the parameter dependencies.

Although the *methods* used in this paper are a generalization of exact analysis methods for scalar $\Sigma\Delta$ modulators in communications theory, much of the current technological *motivation* for the results comes from power electronics. Therefore, while the hexagonal $\Sigma\Delta$ modulator may well find applications outside power electronics, it is appropriate to conclude this introduction with a review of the applications of oversampled analog-to-digital converters to power electronics.

Oversampled analog-to-digital converters have been employed in power electronics for nearly two decades. However, attention to these converters has been sparse in comparison to the vast literature for pulsewidth modulators. The first reported application of an oversampled converter (delta modulator) was to a conventional three-phase transistor inverter wherein the integration of the output voltage was calculated via the output inductors. The output current closed the feedback loop and thus could be controlled [25]. This so-called current controlled delta modulator exhibited a nonzero steady-state output current error, which was improved by the addition of an integrator in the forward path [26].

The invention of the soft switching resonant link converter by Divan [7] fostered interest in $\Sigma\Delta$ modulators since they both require constrained switching instants. Studies of threefold scalar $\Sigma\Delta$ modulators applied to resonant link inverters that considered their spectral performance and harmonic distortion using simulation, experiment, and basic analysis were reported in [27]. The threefold $\Sigma\Delta$ modulator uses three identical independent scalar modulators to control each of the three inverter leg voltages. The threefold modulator has reduced dynamic range compared to the hexagonal $\Sigma\Delta$ modulator. A zero-output voltage state (i.e., all switches high/low) was introduced in [6]

to obtain adjacent state switching. This so-called modified $\Sigma\Delta$ modulator is a threefold $\Sigma\Delta$ modulator with the provision that nonadjacent states are overridden by a zero state. This work differs from the hexagonal $\Sigma\Delta$ in that the zero vector is not chosen unless a nonadjacent state is selected. Seidl [28] derived the hexagonal quantizer based on its one-step ahead optimality properties (minimum-square error) and developed a neural network delta modulator employing the hexagonal quantizer. An alternative to current controlled delta modulators using a one-step ahead minimization of the infinity norm of the current error was proposed in [29]. Attempts to combine $\Sigma\Delta$ modulation with space vector modulation [8] are developed in [30] and [31]. Summaries of the application of current controlled delta modulators and (to a lesser extent) $\Sigma\Delta$ modulators to resonant link inverters prior to 1994 are found in [32], [28], and [30]. A simple coherent analysis of $\Sigma\Delta$ modulators applied to resonant link converters was reported by Mertens in [33]. This work drew from the basic reference in communications for the behavior of quantization noise with dc input of Candy and Benjamin [3]. Recently, Nieznański [34] compared the hexagonal $\Sigma\Delta$ modulator to the modified $\Sigma\Delta$ modulator of [6] and the threefold-scalar $\Sigma\Delta$ modulator [27], [32] and showed that the hexagonal $\Sigma\Delta$ modulator has lower distortion power and device switching rate.

Our conference paper [5] and patent [35] introduced the $\Sigma\Delta$ modulator with hexagonal quantization as well as the extension to double-loop and interpolative $\Sigma\Delta$ modulators. This work represented a significant improvement in spectral performance over prior work and has been implemented in commercial power-electronic products requiring high spectral performance.

A novel insight put forth in [5] is that a power-electronic circuit may be thought of as an analog-to-digital converter in which the analog input is the signal to be synthesized and the quantized digital output is the state of the circuit switches. One consequence of this interpretation is that the power-electronic switching states determine the possible “digitized states” or quantizer outputs. Similarly, other circuits such as the matrix converter, multilevel converters, and multiphase converters define particular quantizer outputs.

II. SINGLE-BIT $\Sigma\Delta$ MODULATOR

This section reviews the spectral calculation for a single-bit $\Sigma\Delta$ modulator with a generic constant input. The results are well known [14], [15], [17], [18]. The purpose of the section is to explain in a simpler context the spectral calculation method that is used for the hexagonal case.

A. Discrete-Time Model

A conventional discrete-time single-loop $\Sigma\Delta$ modulator is shown in Fig. 2 where β , u , $e \in \mathbb{R}$, q is the single-bit quantizer, and the unit delay D with its unity feedback loop is a “discrete-time integrator”

$$q(x) = \begin{cases} \frac{1}{2}, & \text{if } x \geq 0 \\ -\frac{1}{2}, & \text{otherwise.} \end{cases}$$

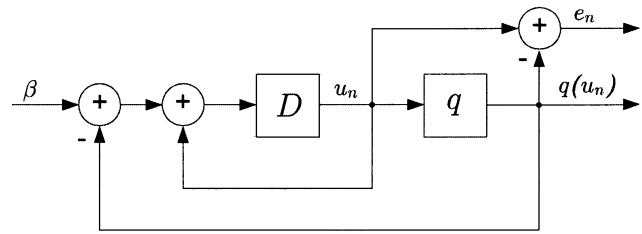


Fig. 2. Discrete-time single-bit or hexagonal $\Sigma\Delta$ modulator. D : unit delay. q : single-bit or hexagonal quantizer.

From Fig. 2, one can write the following difference equations that describe the $\Sigma\Delta$ modulator:

$$u_{n+1} = \beta + u_n - q(u_n) \quad (1)$$

where β is the discrete-time input, u_n is the modulator state, and $q_n = q(u_n)$ is the quantizer output at time n .

A key process in the analysis is the quantizer error sequence defined by

$$e_n = e(u_n) = u_n - q_n. \quad (2)$$

Using (1) and (2), the state and output processes can be expressed in terms of the input and the error sequence

$$u_{n+1} = e_n + \beta \quad (3)$$

$$q_{n+1} = e_n - e_{n+1} + \beta. \quad (4)$$

By substituting (3) into (2), the error sequence satisfies the nonlinear difference equations

$$e_0 = e(u_0) \quad e_{n+1} = e(e_n + \beta), \quad n = 0, 1, \dots \quad (5)$$

B. Solution of the Difference Equation

We assume the no-overload condition that $|\beta| \leq 1/2$ and $|u_0| \leq 1$. It follows that $|e_n| \leq 1/2$ and $|u_n| \leq 1$ for $n = 0, 1, \dots$ [15]. Then, the quantizer error can be expressed as [15]

$$e(u) = \langle u \rangle - \frac{1}{2}, \quad \text{for } u \in [-1, 1] \quad (6)$$

where $\langle r \rangle$ is the fractional part of r ; that is, $\langle r \rangle = r - \lfloor r \rfloor$, where $\lfloor r \rfloor$ denotes the largest integer not greater than r .

For a system with no-overload, (5) becomes

$$e_{n+1} = \langle e_n + \beta \rangle - \frac{1}{2}, \quad n = 0, 1, \dots \quad (7)$$

For convenience, define

$$y_n = y(u_n) = \frac{1}{2} + e(u_n), \quad u_n \in [-1, 1] \quad (8)$$

so that (7) becomes

$$y_{n+1} = \langle y_n + \beta' \rangle, \quad n = 1, 2, \dots \quad (9)$$

where $\beta' = \beta - (1/2)$.

The solution to (9) is [15]

$$y_n = \langle y_0 + n\beta' \rangle. \quad (10)$$

C. Spectrum of the Quantizer Error

The autocorrelation of the y sequence is defined as

$$R_y(n) = \lim_{L \rightarrow \infty} \frac{1}{L} \sum_{k=0}^{L-1} y_k y_{k+n} \quad (11)$$

whenever the limit exists. Use (10) to obtain

$$\begin{aligned} R_y(n) &= \lim_{L \rightarrow \infty} \frac{1}{L} \sum_{k=0}^{L-1} \langle y_0 + k\beta' \rangle \langle y_0 + k\beta' + n\beta' \rangle \\ &= \lim_{L \rightarrow \infty} \frac{1}{L} \sum_{k=0}^{L-1} \langle y_0 + k\beta' \rangle \langle \langle y_0 + k\beta' \rangle + n\beta' \rangle. \end{aligned} \quad (12)$$

A classical result in ergodic theory due to Weyl is [36]

Theorem II.1: If f is a Riemann-integrable function, $\beta \in \mathbb{R}$ is irrational, and $r \in \mathbb{R}$ then

$$\lim_{L \rightarrow \infty} \frac{1}{L} \sum_{k=0}^{L-1} f(\langle bk + r \rangle) = \int_0^1 f(s) ds.$$

We assume β' to be irrational and apply Theorem II.1 to $f(s) = s \langle s + n\beta' \rangle$ in (12) to obtain

$$R_y(n) = \int_0^1 \langle s \rangle \langle s + n\beta' \rangle ds. \quad (13)$$

Let $f, g \in L^2([0, 1])$ have Fourier coefficients $\hat{f}_p, \hat{g}_p, p \in \mathbb{Z}$. Then, Parseval's formula is

$$\int_0^1 f(s) g^*(s) ds = \sum_{p \in \mathbb{Z}} \hat{f}_p \hat{g}_p^*. \quad (14)$$

The function $\langle \cdot \rangle \in L^2([0, 1])$ is periodic and has Fourier series $\langle u \rangle = \sum_{p \in \mathbb{Z}} c_p e^{i2\pi pu}$ where

$$c_p = \int_0^1 \langle u \rangle e^{-i2\pi pu} du = \begin{cases} \frac{1}{2}, & \text{if } p = 0 \\ \frac{i}{2\pi p}, & \text{if } p \neq 0. \end{cases}$$

The Fourier coefficients of $g(x) = \langle x + n\beta' \rangle$ are $c_p e^{i2\pi pn\beta'}$. Applying Parseval's formula to (13) gives

$$R_y(n) = \sum_{p \in \mathbb{Z}} c_p c_p^* e^{-i2\pi pn\beta'} = \sum_{p \in \mathbb{Z}} |c_p|^2 e^{i2\pi pn\beta'}. \quad (15)$$

Since $\sum_{p \in \mathbb{Z}} |c_p|^2 = 1/3$, the series (15) for $R_y(n)$ is absolutely summable and this implies uniform convergence of the series (15) with respect to n . Since almost periodic sequences are the uniform limit of trigonometric polynomials, $R_y(n)$ is almost periodic [37].

We now compute the spectrum S_y of the almost periodic sequence R_y . It is known from harmonic analysis that the spectrum of an almost periodic sequence is discrete (pure point). The pure point part of the spectrum S_y may be recovered from the autocorrelation sequence $R_y(n)$ for any point $\lambda_p \in [0, 1]$ by

the mean value of the almost periodic sequence $R_y(n) e^{-i2\pi \lambda_p n}$ [17], [38]

$$\begin{aligned} S_y(\{\lambda_p\}) &= \lim_{N \rightarrow \infty} \frac{1}{2N+1} \sum_{n=-N}^N R_y(n) e^{-i2\pi \lambda_p n} \\ &= \lim_{N \rightarrow \infty} \frac{1}{2N+1} \sum_{n=-N}^N \sum_{p \in \mathbb{Z}} |c_p|^2 e^{i2\pi(p\beta' - \lambda_p)n} \\ &= \sum_{p \in \mathbb{Z}} |c_p|^2 \lim_{N \rightarrow \infty} \frac{1}{2N+1} \sum_{n=-N}^N e^{i2\pi(p\beta' - \lambda_p)n}. \end{aligned} \quad (16)$$

The interchange of summations is justified since $\sum_{p \in \mathbb{Z}} |c_p|^2 < \infty$. Thus

$$S_y(\{\lambda_p\}) = \begin{cases} 0, & \text{if } p\beta' \neq \lambda_p \pmod{1} \\ |c_p|^2, & \text{if } p\beta' = \lambda_p \pmod{1}. \end{cases} \quad (17)$$

The numbers $\{\lambda_p, p \in \mathbb{Z}\}$ are the Bohr–Fourier frequencies of the sequence $R_y(n)$, and $|c_p|^2$ are the Bohr–Fourier coefficients of $R_y(n)$. Rewriting (17) and using $y = 1/2 + e$ the spectrum of the quantization error is [14], [18]

$$S_e(\omega) = \sum_{\substack{p \in \mathbb{Z} \\ p \neq 0}} |c_p|^2 \delta(\omega - \langle p\beta' \rangle). \quad (18)$$

According to (4), the quantizer output q is obtained by differencing e and adding β . Hence, standard linear-system Fourier-analysis techniques can be applied to obtain from (18) the following spectrum of the quantizer output q :

$$S_q(\omega) = \beta^2 \delta(\omega) + 4 \sum_{\substack{p \in \mathbb{Z} \\ p \neq 0}} |c_p|^2 \sin^2(\pi\omega) \delta(\omega - \langle p\beta' \rangle). \quad (19)$$

The output spectral density S_q is purely discrete having amplitudes $4|c_p|^2 \sin^2(\pi\omega)$ at frequencies $\langle p\beta' \rangle$ for $0 \neq p \in \mathbb{Z}$, and the square of the input at zero frequency.

III. HEXAGONAL $\Sigma\Delta$ MODULATOR

This section describes mathematical underpinnings, including hexagonal coordinate systems, lattices, and quantizers, and states the difference equation for the hexagonal modulator.

A. Hexagonal Lattices and Coordinates

It is convenient to define the plane $\mathcal{P} = \{(x, y, z)^t \in \mathbb{R}^3 \mid x + y + z = 0\}$, where t denotes transpose. Define $W : \mathbb{R}^2 \rightarrow \mathcal{P}$ and $V : \mathcal{P} \rightarrow \mathbb{R}^2$ to be

$$W = \begin{bmatrix} 1 & 0 \\ 0 & 1 \\ -1 & -1 \end{bmatrix} \quad V = \frac{1}{3} \begin{bmatrix} 2 & -1 & -1 \\ -1 & 2 & -1 \end{bmatrix}. \quad (20)$$

VW is the identity on \mathbb{R}^2 and WV is the identity on \mathcal{P} .

The hexagonal lattice is $\Lambda = \bigcup \{Wk \mid k \in \mathbb{Z}^2\} = \mathcal{P} \cap \mathbb{Z}^3$. The large dots in Fig. 3 show points in Λ .

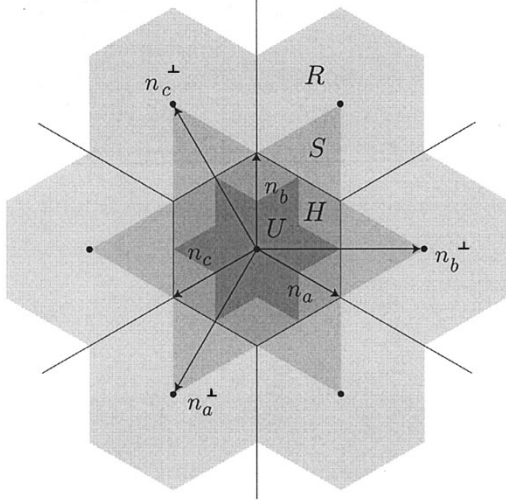


Fig. 3. Hexagonal quantizer q and regions H , S , and R .

The dual of \mathcal{P} is $\mathcal{P}^* = \{(x, y, z) \in \mathbb{R}^{*3} \mid x + y + z = 0\}$. The lattice *dual* [9] to Λ is

$$\Lambda^* = \{p \in \mathcal{P}^* \mid p\lambda \in \mathbb{Z} \text{ for all } \lambda \in \Lambda\} = \bigcup \{qV \mid q \in \mathbb{Z}^{*2}\}.$$

The vertices of hexagon H in Fig. 3 are points in Λ^* .

Vectors in \mathcal{P} or Λ are written as column vectors and dual vectors in \mathcal{P}^* or Λ^* are written as row vectors. For example, $n_a \in \mathcal{P}$ in Fig. 3 is the column vector $1/3(2, -1, -1)^t$. The columns of W generate Λ and the rows of V generate Λ^* .

The Voronoi cells (points closest to a given lattice point) of Λ are hexagons of side $\sqrt{2/3}$. Define the set H to be the interior of the Voronoi cell containing 0, together with a specific choice of three nonopposite hexagon sides and two opposite hexagon vertices. (These choices ensure that lattice translates of H tile the plane with no overlapping points.) H is the dark central hexagonal region of Fig. 3. The area of H is $|H| = \sqrt{3}$.

Define vectors n and n^\perp by (see Fig. 3)

$$\begin{aligned} n_a &= \frac{1}{3} \begin{pmatrix} 2 \\ -1 \\ -1 \end{pmatrix} & n_b &= \frac{1}{3} \begin{pmatrix} -1 \\ 2 \\ -1 \end{pmatrix} & n_c &= \frac{1}{3} \begin{pmatrix} -1 \\ -1 \\ 2 \end{pmatrix} \\ n_a^\perp &= \begin{pmatrix} 0 \\ -1 \\ 1 \end{pmatrix} & n_b^\perp &= \begin{pmatrix} 1 \\ 0 \\ -1 \end{pmatrix} & n_c^\perp &= \begin{pmatrix} -1 \\ 1 \\ 0 \end{pmatrix}. \end{aligned}$$

Also define $n_{-s} = -n_s$, $n_{-s}^\perp = -n_s^\perp$. Note that $n_s^t n_s^\perp = 0$, $|n^\perp| = \sqrt{2}$, and $|n| = \sqrt{2/3}$.

Coordinates $\beta_a^\perp, \beta_b^\perp, \beta_c^\perp$ for \mathcal{P} are defined by

$$\beta_a^\perp = \beta \cdot n_a^\perp \quad \beta_b^\perp = \beta \cdot n_b^\perp \quad \beta_c^\perp = \beta \cdot n_c^\perp. \quad (21)$$

Coordinates p_a, p_b, p_c for \mathcal{P}^* are defined by

$$p_a = pn_a \quad p_b = pn_b \quad p_c = pn_c. \quad (22)$$

It is convenient to define an ordered coordinate system for \mathcal{P} . Let $\beta_1^\perp, \beta_2^\perp, \beta_3^\perp$ be an ordering of $\beta_a^\perp, \beta_b^\perp, \beta_c^\perp$ chosen so that

$|\beta_1^\perp| \geq |\beta_2^\perp| \geq |\beta_3^\perp|$. The ordered coordinates are a continuous nondifferentiable function of the original coordinates. Also, the ordered coordinates satisfy the relation

$$|\beta_1^\perp| = |\beta_2^\perp| + |\beta_3^\perp|. \quad (23)$$

Equation (23) is proved by noting that when β_1^\perp is positive (say), β_2^\perp and β_3^\perp are necessarily negative; and that $\beta_1^\perp + \beta_2^\perp + \beta_3^\perp = 0$. We write $n_j^\perp = \beta_j^\perp / |\beta_j^\perp|$, $j = 1, 2, 3$ so that $\beta_j^\perp = \beta \cdot n_j^\perp$.

In the ordered coordinate system we may define with economy the various regions of Fig. 3

$$H = \{x \in \mathcal{P} : |x_1^\perp| \leq 1\} \quad (24)$$

$$U = \left\{x \in \mathcal{P} : |x_2^\perp| \leq \frac{1}{2}\right\} \quad (25)$$

$$S = \{x \in \mathcal{P} : |x_2^\perp| \leq 1\} \quad (26)$$

$$R = \{x \in \mathcal{P} : |x_1^\perp| \leq 3 \text{ and } |x_2^\perp| \leq 2\}. \quad (27)$$

B. Hexagonal Quantizer and Discrete-Time Model

A function f on \mathcal{P} is *hexagonally periodic* if $f(x+\lambda) = f(x)$ for all $\lambda \in \Lambda$. Define $\langle \cdot \rangle : \mathcal{P} \rightarrow H$ as the identity on H and extend the definition of $\langle \cdot \rangle$ to \mathcal{P} by making $\langle \cdot \rangle$ hexagonally periodic. One might call $\langle \cdot \rangle$ “hexagonal part” since $\langle \cdot \rangle$ generalizes the scalar fractional part $\langle \cdot \rangle$.

Let $x, y \in \mathcal{P}$. Then

$$\langle x+y \rangle = \langle \langle x \rangle + y \rangle. \quad (28)$$

Define the hexagonal lattice nearest neighbor quantization function q to be

$$q(x) = x - \langle x \rangle. \quad (29)$$

The nearest neighbor quantizer q is shown in Fig. 3. The input u to q is a point in the plane \mathcal{P} and the output $q(u)$ is the nearest to u of the 7 truncated hexagonal lattice points $\{0, \pm n_a^\perp, \pm n_b^\perp, \pm n_c^\perp\}$ in Fig. 3.

A discrete-time hexagonal $\Sigma\Delta$ modulator is shown in Fig. 2. The signals β, u_n, q_n , and e_n are now interpreted as vectors in the plane \mathcal{P} .

The discrete-time model derivation exactly parallels that of Section II-A and the error sequence satisfies the nonlinear difference equations

$$e_0 = e(u_0) \quad e_{n+1} = e(e_n + \beta), \quad n = 0, 1, 2, \dots \quad (30)$$

C. Solution of the Difference Equation

Our analysis requires the modulator state u_n , $n = 0, 1, 2, \dots$ to be contained in the no-overload region R of the quantizer. R is the lightly shaded region of Fig. 3 consisting of the seven hexagons closest to zero. S is the star-shaped shaded region of Fig. 3. The following sufficient condition for no-overload can be shown by induction. If $\beta \in S$ and $e_0 \in H$, then $e_n \in H$ and $u_n \in R$ for all $n = 0, 1, 2, \dots$. We assume $\beta \in S$ and $e_0 \in H$ and hence no-overload for the rest of the paper.

Since the function $e(u) = u - q(u)$ coincides with $\langle \cdot \rangle$ on the no-overload region R , the no-overload assumption implies that the difference equation (30) can be written as

$$e_{n+1} = \langle e_n + \beta \rangle. \quad (31)$$

Property (28) can be used to check that the solution to (31) is

$$e_n = \langle e_0 + n\beta \rangle. \quad (32)$$

D. Fourier and Ergodic Results

We state results about Fourier analysis and ergodic shifts. Let $f, g : \mathcal{P} \rightarrow \mathbb{C}$ be hexagonally periodic and Lebesgue square integrable on H . Then, $f(x) = \sum_{p \in \Lambda^*} \hat{f}_p e^{i2\pi p x}$ where the equality is in the L^2 sense and the Fourier coefficients are $\hat{f}_p = (1/|H|) \int_H f(s) e^{-i2\pi p s} ds$. Parseval's formula is

$$\frac{1}{|H|} \int_H f(s) g^*(s) ds = \sum_{p \in \Lambda^*} \hat{f}_p \hat{g}_p^*. \quad (33)$$

These Fourier results can be obtained either as sketched in Appendix I or as a particular case of harmonic analysis on compact Abelian groups [39].

Identify points of \mathcal{P} differing by vectors in Λ to define $\mathcal{H} = \mathcal{P}/\Lambda = \{x + \Lambda \mid x \in \mathcal{P}\}$. \mathcal{H} is a compact Abelian group. A function $f : H \rightarrow \mathbb{C}$ lifts to a function $\tilde{f} : \mathcal{H} \rightarrow \mathbb{C}$ if $\tilde{f}(x + \Lambda) = f(x)$ for all x . Lemma III.1 gives a generic condition on the input β for the dynamics (32) to induce a uniquely ergodic shift on \mathcal{H} so that time averages of a function f can be evaluated as an integral over H .

Lemma III.1: Let $\beta \in \mathcal{P}$ be such that the only $p \in \Lambda^*$ with $p\beta \in \mathbb{Z}$ is $p = 0$. Let $f : H \rightarrow \mathbb{R}$ have a continuous lifting $\tilde{f} : \mathcal{H} \rightarrow \mathbb{R}$. Then, for all $e_0 \in \mathcal{P}$

$$\lim_{L \rightarrow \infty} \frac{1}{L} \sum_{n=0}^{L-1} f(\langle e_0 + n\beta \rangle) = \frac{1}{|H|} \int_H f(s) ds.$$

Corollary III.1: Lemma III.1 extends to functions $f : H \rightarrow \mathbb{R}$ for which there exist sequences of functions $\bar{f}_k, \underline{f}_k, k = 1, 2, \dots$ with continuous liftings such that $\underline{f}_k(x) \leq f(x) \leq \bar{f}_k(x)$ for all x and $|\underline{f}_k - \bar{f}_k|_\infty \rightarrow 0$ as $k \rightarrow \infty$.

Lemma III.1 can be obtained from standard results on the torus [40] as indicated in Appendix I.

IV. SPECTRAL ANALYSIS

This section computes the power-spectral density of the quantizer error function and the quantizer output for the hexagonal $\Sigma\Delta$ modulator with a constant input. There are three cases to consider, depending on the value of the constant input β . These three cases generalize the cases β irrational and β rational for the single-bit modulator.

Case 1: $\{s \in \Lambda^* \mid s\beta \in \mathbb{Z}\} = \{0\}$. In Case 1, the error sequence e_n described by (32) is equidistributed over H so that Lemma III.1 applies. Case 1 is the generic case satisfied by $\beta \in H$ almost everywhere.

Case 2: $\{s \in \Lambda^* \mid s\beta \in \mathbb{Z}\} = \{mr \mid m \in \mathbb{Z}\}$ for some nonzero $r \in \Lambda^*$. Another characterization of Case 2 is that β has the form

$$\beta = \alpha r_\perp + \frac{z}{g} \sigma, \quad r_\perp \in \Lambda; \quad \sigma \in \Lambda; \quad z \in \mathbb{Z}; \quad g \in \mathbb{Z} \quad (34)$$

where $\alpha \in \mathbb{R}$ is irrational and $r_\perp \neq 0$. In Case 2, the sequence e_n described by (32) is confined to lines in H , but the sequence is aperiodic and equidistributed over the lines.

Case 3: β has the form

$$\beta = \frac{h}{q} v, \quad v \in \Lambda; \quad h \in \mathbb{Z}; \quad q \in \mathbb{Z} \quad (35)$$

where h and q are relatively prime. In Case 3, the sequence e_n described by (32) is confined to discrete points in H and is periodic with period q .

The Case 1–3 characterizations are proved in Appendix II.

A. Autocorrelation Computation

The autocorrelation matrix of the noise is, using (32)

$$\begin{aligned} R_e(k) &= \lim_{L \rightarrow \infty} \frac{1}{L} \sum_{n=0}^{L-1} e_n \otimes e_{n+k} \\ &= \lim_{L \rightarrow \infty} \frac{1}{L} \sum_{n=0}^{L-1} \langle e_0 + n\beta \rangle \otimes \langle e_0 + n\beta + k\beta \rangle \end{aligned} \quad (36)$$

where \otimes denotes outer product. The following three subsections compute the autocorrelation in Cases 1, 2, and 3 starting from (36).

1) Autocorrelation Computation Case 1: Case 1 is the generic case in which Lemma III.1 applies and the calculation proceeds as a generalization of the method for the single-bit modulator presented in Section II.

Equation (36) may be modified using (28) to give

$$R_e(k) = \lim_{L \rightarrow \infty} \frac{1}{L} \sum_{n=0}^{L-1} \langle e_0 + n\beta \rangle \otimes \langle \langle e_0 + n\beta \rangle + k\beta \rangle.$$

Define $f : H \rightarrow \mathcal{P} \times \mathcal{P}$ by $f(s) = s \otimes \langle s + k\beta \rangle$. Then

$$R_e(k) = \lim_{L \rightarrow \infty} \frac{1}{L} \sum_{n=0}^{L-1} f(\langle e_0 + n\beta \rangle).$$

Each component of f is continuous except on several line segments and satisfies the conditions of Corollary III.1. Hence

$$R_e(k) = \frac{1}{|H|} \int_H \langle s \rangle \otimes \langle s + k\beta \rangle ds. \quad (37)$$

Let c_p be the Fourier coefficients of $\langle \cdot \rangle$ for $p \in \Lambda^*$

$$c_p = \frac{1}{|H|} \int_H \langle s \rangle e^{-i2\pi p s} ds. \quad (38)$$

Appendix III computes c_p as

$$c_p = \frac{-i \operatorname{sgn}(p) p^t}{4\sqrt{3}\pi^2 \Pi(p)} \quad (39)$$

where Π and sgn are defined as follows. Using coordinates (22) so that $p = (p_a, p_b, p_c)$, define

$$\begin{aligned} \Pi(p) &= \text{product of nonzero elements of } \{p_a, p_b, p_c\}; p \neq 0 \\ \Pi(0) &= 1. \end{aligned}$$

Partition $\Lambda^* = \Lambda^t \cup (n_a^t + \Lambda^t) \cup (-n_a^t + \Lambda^t)$ and define

$$\operatorname{sgn}(p) = \begin{cases} 0, & \text{if } p \in \Lambda^t; \quad p_a p_b p_c \neq 0; \quad \text{or } p = 0 \\ \frac{2\pi}{\sqrt{3}}, & \text{if } p \in \Lambda^t; \quad p_a p_b p_c = 0; \quad \text{and } p \neq 0 \\ 1, & \text{if } p \in n_a^t + \Lambda^t \\ -1, & \text{if } p \in -n_a^t + \Lambda^t. \end{cases}$$

The Fourier coefficients of $f(x) = \langle x + k\beta \rangle$ are $c_p e^{i2\pi p\beta k}$.

Each entry of the outer product in (37) can be regarded as an inner product of functions over H and applying Parseval's formula (33) to each entry gives

$$R_e(k) = \sum_{p \in \Lambda^*} c_p \otimes c_{-p} e^{-i2\pi p\beta k}. \quad (40)$$

2) *Autocorrelation Computation Case 2:* Recall from (34) that in Case 2, $\beta = \alpha r_\perp + (z/g)\sigma$ where $r_\perp, \sigma \in \Lambda$ and $z, g \in \mathbb{Z}$ and $\alpha \in \mathbb{R}$ is irrational. Equation (36) for the autocorrelation matrix may be rewritten as

$$\begin{aligned} R_e(k) &= \lim_{L' \rightarrow \infty} \frac{1}{L'} \sum_{n=0}^{L'-1} f\left(\langle n\beta + e_0 \rangle\right) \\ &= \lim_{L \rightarrow \infty} \frac{1}{gL} \sum_{n=0}^{L-1} \sum_{m=0}^{g-1} f\left(\langle (ng+m)\beta + e_0 \rangle\right) \\ &= \frac{1}{g} \sum_{m=0}^{g-1} \lim_{L \rightarrow \infty} \frac{1}{L} \sum_{n=0}^{L-1} f\left(\langle ng\alpha + m\alpha \rangle r_\perp + \frac{mz}{g}\sigma + e_0\right). \end{aligned}$$

Use α irrational and Weyl's ergodic theorem II.1 to get

$$\begin{aligned} R_e(k) &= \frac{1}{g} \sum_{m=0}^{g-1} \int_0^1 f\left(\langle \theta r_\perp + \frac{mz}{g}\sigma + e_0 \rangle\right) d\theta \\ &= \frac{1}{g} \sum_{m=0}^{g-1} \int_0^1 \langle \theta r_\perp + \frac{mz}{g}\sigma + e_0 \rangle \\ &\quad \otimes \langle \theta r_\perp + \frac{mz}{g}\sigma + k\beta + e_0 \rangle d\theta. \end{aligned} \quad (41)$$

The Fourier coefficients of the factors inside the integral in (41) can be obtained from their Fourier expansions, e.g.,

$$\begin{aligned} \langle \theta r_\perp + \frac{mz}{g}\sigma + e_0 \rangle &= \sum_{p \in \Lambda^*} c_p e^{i2\pi(\theta p r_\perp + (mz/g)p\sigma + p e_0)} \\ &= \sum_{n \in \mathbb{Z}} \sum_{\substack{p \in \Lambda^* \\ p r_\perp = n}} c_p e^{i2\pi((mz/g)p\sigma + p e_0)} e^{i2\pi n \theta}. \end{aligned}$$

Applying Parseval's formula (14) to (41) gives

$$\begin{aligned} R_e(k) &= \frac{1}{g} \sum_{m=0}^{g-1} \sum_{n \in \mathbb{Z}} \sum_{\substack{p \in \Lambda^* \\ p r_\perp = n}} c_p e^{i2\pi((mz/g)p\sigma + p e_0)} \\ &\quad \otimes \sum_{\substack{p' \in \Lambda^* \\ p' r_\perp = n}} c_{p'} e^{-i2\pi((mz/g)p'\sigma + k p' \beta + p' e_0)}. \end{aligned} \quad (42)$$

According to Appendix IV, the summations in (42) are absolutely convergent and can be reordered to give

$$\begin{aligned} R_e(k) &= \sum_{n \in \mathbb{Z}} \sum_{\substack{p, p' \in \Lambda^* \\ p r_\perp = n \\ p' r_\perp = n}} c_p \otimes c_{-p'} e^{-i2\pi k p' \beta} \\ &\quad \cdot \frac{1}{g} \sum_{m=0}^{g-1} e^{i2\pi(mz/g)(p-p')\sigma} e^{i2\pi(p-p')e_0} \\ &= \sum_{\substack{p, p' \in \Lambda^* \\ (p-p')r_\perp = 0 \\ (p-p')\sigma = 0 \pmod{g}}} c_p \otimes c_{-p'} e^{-i2\pi k p' \beta} e^{i2\pi(p-p')e_0} \end{aligned} \quad (43)$$

$$= \sum_{\substack{p, p' \in \Lambda^* \\ (p-p')\beta \in \mathbb{Z}}} c_p \otimes c_{-p'} e^{-i2\pi k p' \beta} e^{i2\pi(p-p')e_0} \quad (44)$$

$$= \sum_{\substack{p, s \in \Lambda^* \\ s\beta \in \mathbb{Z}}} c_p \otimes c_{s-p} e^{i2\pi k p \beta} e^{i2\pi s e_0}. \quad (45)$$

The equivalence of (43) and (44) follows from (77) in Appendix II.

3) *Autocorrelation Computation Case 3:* Recall from (35) that in Case 3, $\beta = (h/q)v$ where $v \in \Lambda$ and $h, q \in \mathbb{Z}$ are relatively prime. Then (36) may be rewritten as

$$R_e(k) = \frac{1}{q} \sum_{m=0}^{q-1} \langle \frac{m}{q}v + e_0 \rangle \otimes \langle \frac{m}{q}v + k\beta + e_0 \rangle. \quad (46)$$

The Fourier coefficients of the factors inside the sum in (46) can be obtained from their Fourier expansions, e.g.,

$$\begin{aligned} \langle \frac{m}{q}v + e_0 \rangle &= \sum_{p \in \Lambda^*} c_p e^{i2\pi((m/q)pv + p e_0)} \\ &= \sum_{n=0}^{q-1} \sum_{\substack{p \in \Lambda^* \\ pv = n \pmod{q}}} c_p e^{i2\pi p e_0} e^{i2\pi n m / q}. \end{aligned}$$

Applying Parseval's formula for scalar discrete periodic functions to (46) gives

$$\begin{aligned}
R_e(k) &= \sum_{n=0}^{q-1} \sum_{\substack{p' \in \Lambda^* \\ p'v=n(\bmod q)}} c_p e^{i2\pi p e_0} \\
&\quad \otimes \sum_{\substack{p' \in \Lambda^* \\ p'v=n(\bmod q)}} c_{p'}^* e^{-i2\pi(kp'\beta + p'e_0)} \\
&= \sum_{n=0}^{q-1} \sum_{\substack{p, p' \in \Lambda^* \\ pv=n(\bmod q) \\ p'v=n(\bmod q)}} c_p \otimes c_{-p'} e^{-i2\pi kp'\beta} e^{i2\pi(p-p')e_0} \\
&= \sum_{\substack{p, p' \in \Lambda^* \\ (p-p')v=0(\bmod q)}} c_p \otimes c_{-p'} e^{-i2\pi kp'\beta} e^{i2\pi(p-p')e_0} \\
&= \sum_{\substack{p, p' \in \Lambda^* \\ (p-p')\beta \in \mathbb{Z}}} c_p \otimes c_{-p'} e^{-i2\pi kp'\beta} e^{i2\pi(p-p')e_0} \\
&= \sum_{\substack{p, s \in \Lambda^* \\ s\beta \in \mathbb{Z}}} c_p \otimes c_{s-p} e^{i2\pi kp\beta} e^{i2\pi s e_0}. \tag{47}
\end{aligned}$$

B. Formal Derivation of Autocorrelation

As a supplement to the rigorous derivation above, we give a formal derivation of the autocorrelation that neglects issues of convergence and interchange of infinite operations. The purpose is to show the commonality between the three cases. Starting from (36)

$$\begin{aligned}
R_e(k) &= \lim_{L \rightarrow \infty} \frac{1}{L} \sum_{n=0}^{L-1} \\
&\quad \sum_{p \in \Lambda^*} c_p e^{i2\pi(np\beta + pe_0)} \otimes \sum_{p' \in \Lambda^*} c_{p'} e^{i2\pi((n+k)p'\beta + p'e_0)} \\
&= \sum_{p, p' \in \Lambda^*} c_p \otimes c_{p'} e^{i2\pi kp'\beta} e^{i2\pi(p+p')e_0} \\
&\quad \cdot \lim_{L \rightarrow \infty} \frac{1}{L} \sum_{n=0}^{L-1} e^{i2\pi n\theta(p+p')\beta} \\
&= \sum_{\substack{p, p' \in \Lambda^* \\ (p+p')\beta \in \mathbb{Z}}} c_p \otimes c_{p'} e^{i2\pi kp'\beta} e^{i2\pi(p+p')e_0} \\
&= \sum_{\substack{p, s \in \Lambda^* \\ s\beta \in \mathbb{Z}}} c_p \otimes c_{s-p} e^{-i2\pi kp\beta} e^{i2\pi s e_0}. \tag{48}
\end{aligned}$$

In Case 1, (48) reduces to the rigorously derived (40) since $s\beta \in \mathbb{Z}$ for $s \in \Lambda^*$ implies $s = 0$ in Case 1. Moreover in Cases 2 and 3, (48) is the same as (45) and (47).

C. Spectrum of Error and Output Sequence

According to (40), (45), and (47) for Cases 1, 2, and 3 the autocorrelation matrix has the general form

$$R_e(k) = \sum_{\substack{p, s \in \Lambda^* \\ s\beta \in \mathbb{Z}}} c_p \otimes c_{s-p} e^{i2\pi s e_0} e^{-i2\pi p\beta k}. \tag{49}$$

The absolute summability of the series (49) is proved in Appendix IV and this implies uniform convergence of (49) with respect to k . Since almost periodic sequences are the uniform limit of trigonometric polynomials, we conclude that each matrix element of $R_e(k)$ is almost periodic [37].

Similarly to the scalar case, the Bohr–Fourier series (49) implies that the quantization error spectral matrix S_e is purely discrete having amplitudes $\sum_{\substack{s \in \Lambda^* \\ s\beta \in \mathbb{Z}}} c_p \otimes c_{s-p} e^{i2\pi s e_0}$ at frequencies $\langle p\beta \rangle$ for $p \in \Lambda^*$

$$S_e(\omega) = \sum_{p \in \Lambda^*} \sum_{\substack{s \in \Lambda^* \\ s\beta \in \mathbb{Z}}} c_p \otimes c_{s-p} e^{i2\pi s e_0} \delta(\omega - \langle p\beta \rangle). \tag{50}$$

Note that the amplitudes are real because c_p and c_{s-p} are both imaginary [see (39)] so that $c_p \otimes c_{s-p}$ is real and because of the symmetry of the sum over s . In particular, $s\beta \in \mathbb{Z} \iff -s\beta \in \mathbb{Z}$.

The quantizer output q_n is obtained by differencing e_n and adding β according to (4). Hence, the output spectral density matrix is

$$S_q(\omega) = \beta \otimes \beta \delta(\omega) + 4 \sin^2(\pi\omega) S_e(\omega). \tag{51}$$

Now we examine some of the special forms of these spectra in the Cases 1, 2, and 3 described in Section IV.

1) *Spectra in Case 1:* For generic input β satisfying Case 1, the error spectrum (50) reduces to

$$S_e(\omega) = \sum_{p \in \Lambda^*} c_p \otimes c_{-p} \delta(\omega - \langle p\beta \rangle) \tag{52}$$

and the output spectrum (51) becomes

$$\beta \otimes \beta \delta(\omega) + \sum_{p \in \Lambda^*} \frac{\sin^2(\pi\omega) \operatorname{sgn}^2(p)}{12\pi^4 \Pi^2(p)} p \otimes p \delta(\omega - \langle p\beta \rangle).$$

Hence, the frequencies and, therefore, the amplitudes of the spectra depend strongly on the input β . Clearly, the spectrum is far from white noise being neither white nor continuous. The error and the output are quasi-periodic.

2) *Spectra in Case 2:* Recall from (34) that in Case 2, $\beta = \alpha r_\perp + (z/g)\sigma$ where $r_\perp, \sigma \in \Lambda$ and $z, g \in \mathbb{Z}$ and $\alpha \in \mathbb{R}$ is irrational. Moreover, $\{s \in \Lambda^* \mid s\beta \in \mathbb{Z}\} = \{mr \mid m \in \mathbb{Z}\}$. Then, the error spectrum (50) can be written as

$$\sum_{p \in \Lambda^*} \sum_{m \in \mathbb{Z}} c_p \otimes c_{mr-p} e^{i2\pi m r e_0} \delta\left(\omega - \left\langle \alpha p r_\perp + \frac{z}{g} p \sigma \right\rangle\right).$$

3) *Spectra in Case 3:* Recall from (35) that in Case 3, $\beta = (h/q)v$ where $v \in \Lambda$ and $h, q \in \mathbb{Z}$. Then, the error spectrum (50) can be written as

$$S_e(\omega) = \sum_n \sum_{\substack{p, s \in \Lambda^* \\ pv=n(\bmod q) \\ sv=0(\bmod q)}} c_p \otimes c_{s-p} e^{i2\pi s e_0} \delta\left(\omega - \left\langle \frac{hn}{q} \right\rangle\right)$$

showing that frequencies are equally spaced at multiples of $1/q$. The output spectrum frequencies are spaced in the same way. The error and the output have period q .

V. MEAN AND VARIANCE

This section computes the mean and variance of the quantizer error in Case 1 of a generic constant input.

Using (32) and Lemma III.1, the mean \bar{e} of the noise is

$$\begin{aligned} \lim_{L \rightarrow \infty} \frac{1}{L} \sum_{n=0}^{L-1} e_n &= \lim_{L \rightarrow \infty} \frac{1}{L} \sum_{n=0}^{L-1} \langle e_0 + n\beta \rangle \\ &= \frac{1}{|H|} \int_H s \, ds \\ &= 0. \end{aligned}$$

The quantizer output q is obtained by differencing e and adding β according to (4). Hence, as expected, the mean quantizer output is $\bar{q} = \beta$.

The covariance matrix σ_e^2 of the quantizer error is $R_e(0)$, the autocorrelation matrix evaluated at zero. Calculation of $R_e(0)$ from (37) is straightforward [9]

$$\sigma_e^2 = \frac{1}{|H|} \int_H s \otimes s \, ds = \frac{5}{36} \frac{1}{3} \begin{bmatrix} 2 & -1 & -1 \\ -1 & 2 & -1 \\ -1 & -1 & 2 \end{bmatrix}.$$

The variance of one component of e is $10/108 = 0.0926$.

VI. AVERAGE SWITCHING RATE

A. Single-Bit $\Sigma\Delta$ Modulator

We derive the average switching rate for the single-bit $\Sigma\Delta$ modulator with the assumptions of no-overload and constant irrational input β .

First use (4) and notation from section Section II-B to show that

$$\begin{aligned} q_{n+1} - q_n &= -e_{n+1} + 2e_n - e_{n-1} \\ &= -\langle e_n + \beta \rangle + 2e_n - \langle e_n - \beta \rangle \\ &= \lfloor e_n + \beta \rfloor + \lfloor e_n - \beta \rfloor. \end{aligned}$$

The condition for no switching between n and $n+1$ is

$$q_{n+1} = q_n \iff \lfloor e_n + \beta \rfloor + \lfloor e_n - \beta \rfloor = 0.$$

Write χ for the indicator function, so that the average switching rate f_s is given by

$$\begin{aligned} 1 - f_s &= \lim_{L \rightarrow \infty} \frac{1}{L} \sum_{n=0}^{L-1} \chi[\text{no switching between } n, n+1] \\ &= \lim_{L \rightarrow \infty} \frac{1}{L} \sum_{n=0}^{L-1} \chi[\lfloor e_n + \beta \rfloor + \lfloor e_n - \beta \rfloor = 0] \\ &= \int_0^1 \chi[\lfloor s + \beta \rfloor + \lfloor s - \beta \rfloor = 0] \, ds \end{aligned} \quad (53)$$

by Theorem II.1. By inspection (53) is

$$f_s = \begin{cases} 2\beta, & 0 \leq \beta < \frac{1}{2} \\ 2(1 - \beta), & \frac{1}{2} \leq \beta < 1. \end{cases} \quad (54)$$

The maximum switching rate $f_s = 1$ occurs at $\beta = 1/2$.

B. Hexagonal $\Sigma\Delta$ Modulator

We derive the switching rate for the hexagonal $\Sigma\Delta$ modulator with constant input vector $\beta \in S$ (see Fig. 3). No-overload and generic β satisfying Case 1 are assumed.

First, use (4), (28), and the definition of q in Section III-B to show that

$$\begin{aligned} q_{n+1} - q_n &= -e_{n+1} + 2e_n - e_{n-1} \\ &= -\langle e_n + \beta \rangle + 2e_n - \langle e_n - \beta \rangle \\ &= q(e_n + \beta) + q(e_n - \beta). \end{aligned}$$

The condition for no switching between n and $n+1$ is

$$\begin{aligned} q_{n+1} = q_n &\iff q(e_n + \beta) + q(e_n - \beta) = 0 \\ &\iff q(e_n + \beta) = 0 \quad \text{and} \quad q(e_n - \beta) = 0 \end{aligned} \quad (55)$$

since $0 \neq q(e_n + \beta) = -q(e_n - \beta)$ is impossible. Write $H + \beta$ for the hexagon H translated by β so that (55) may be written as $e_n \in H - \beta$ and $e_n \in H + \beta$. Then, the condition for no switching between n and $n+1$ is

$$e_n \in (H - \beta) \cap (H + \beta). \quad (56)$$

Using Corollary III.1, the average switching rate f_s is

$$\begin{aligned} 1 - f_s &= \lim_{L \rightarrow \infty} \frac{1}{L} \sum_{n=0}^{L-1} \chi[\text{no switching between } n, n+1] \\ &= \lim_{L \rightarrow \infty} \frac{1}{L} \sum_{n=0}^{L-1} \chi[e_n \in (H - \beta) \cap (H + \beta)] \\ &= \frac{1}{|H|} \int_H \chi[s \in (H - \beta) \cap (H + \beta)] \, ds \\ &= \frac{1}{|H|} \text{Area}[(H - \beta) \cap (H + \beta)]. \end{aligned} \quad (57)$$

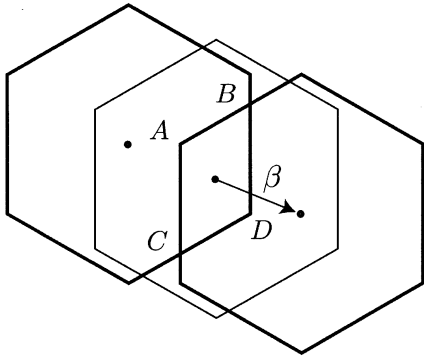
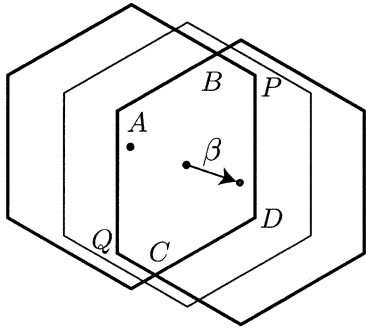
Equation (57) relates f_s to the overlapping area of two shifted hexagons as shown in Figs. 4 and 5. This is a useful geometric interpretation. For instance, we immediately see that f_s is maximum for β on the perimeter of H . To compute the area (57) for $\beta \in S$, there are three cases.

Case A: $\beta \in U^c \cap H$. Consider the particular case of β in the lower half of the n_b^+ sextant as shown in Fig. 4. According to (57), the switching rate is

$$f_s = 1 - \frac{1}{|H|} \text{Area}(ABDC) = 1 - \frac{\sqrt{3}}{2|H|} |AB| |BD|. \quad (58)$$

By computing the positions of A, B, D in terms of the vertices of H and β , it can be shown that $|AB| = -2(\beta_b^+ - 1)|n|$ and $|BD| = 2(\beta_c^+ + 1)|n|$. Hence

$$\begin{aligned} f_s &= 1 + \frac{4}{3}(\beta_b^+ - 1)(\beta_c^+ + 1) \\ &= -\frac{1}{3} + \frac{4}{3}(|\beta_b^+| + |\beta_c^+| - |\beta_b^+||\beta_c^+|). \end{aligned}$$

Fig. 4. Overlap of two shifted hexagons for $\beta \in U^c \cap H$.Fig. 5. Overlap of two shifted hexagons for $\beta \in U$.

Using the ordered coordinates described in Section III, the general case for any $\beta \in U^c \cap H$ is

$$f_s = -\frac{1}{3} + \frac{4}{3} (|\beta_1^\perp| + |\beta_2^\perp| - |\beta_1^\perp||\beta_2^\perp|). \quad (59)$$

Case B: $\beta \in U$. Consider the particular case of β in the lower half of the n_b^\perp sextant as shown in Fig. 5. The switching rate is

$$\begin{aligned} f_s &= 1 - \frac{1}{|H|} \text{Area}(ABPDCQ) \\ &= 1 - \frac{1}{|H|} \left(|BP||BQ| + \frac{\sqrt{3}}{2} |AB||AQ| \right). \end{aligned}$$

By computing the positions of A, B, P, Q , it can be shown that $|BP| = |n|(2\beta_c^\perp + 1)$, $|BQ| = |n^\perp|(\beta_a^\perp + 1)$, $|AB| = |n|(2\beta_a^\perp + 1)$, and $|AQ| = |n|$. Hence

$$\begin{aligned} f_s &= -\frac{4}{3} (\beta_c^\perp + \beta_a^\perp + \beta_c^\perp \beta_a^\perp) \\ &= \frac{4}{3} (|\beta_c^\perp| + |\beta_a^\perp| - |\beta_c^\perp||\beta_a^\perp|). \end{aligned}$$

The general case for any $\beta \in U$ is, using (23)

$$\begin{aligned} f_s &= \frac{4}{3} (|\beta_2^\perp| + |\beta_3^\perp| - |\beta_2^\perp||\beta_3^\perp|) \\ &= \frac{4}{3} (|\beta_1^\perp| - |\beta_2^\perp||\beta_3^\perp|). \end{aligned} \quad (60)$$

Case C: $\beta \in H^c \cap S$. Since (57) is a function of $\widehat{\beta}$, the average switching rate at $\beta \in H^c \cap S$ is equal to the average switching rate at $\widehat{\beta} = \beta - q(\beta) \in H$.

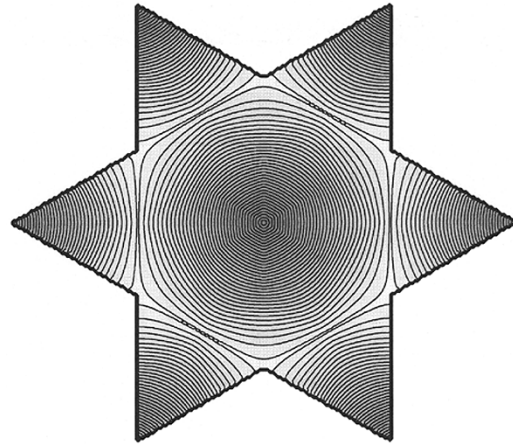
Fig. 6. Switching-rate contour plot over region S .

Fig. 6 shows a contour plot of the switching rate evaluated with (59) and (60). The switching rate is zero at the origin and has its maximum value of one on the perimeter of H . For small β , the product term in (60) is negligible and hence the contours are approximately hexagonal near the origin.

C. Slowly Varying Sinusoidal Inputs

We determine the switching rate for sinusoidal inputs that are slowly varying with respect to the switching rate. Sinusoidal inputs correspond to circles in the plane \mathcal{P} and the circle radius is proportional to the sinusoidal input amplitude. This subsection computes the average switching rate on circles as the radius is varied and then quantifies the deviations of the switching rate from the average switching rate as the circle is traversed.

To describe the circles, it is convenient to use polar coordinates (r, θ) in the plane \mathcal{P} . The transformation to coordinates (21) is

$$\begin{pmatrix} \beta_a^\perp \\ \beta_b^\perp \\ \beta_c^\perp \end{pmatrix} = \begin{bmatrix} -1 & \sqrt{3} \\ 2 & 0 \\ -1 & -\sqrt{3} \end{bmatrix} \begin{pmatrix} r \cos \theta \\ r \sin \theta \end{pmatrix}. \quad (61)$$

For example, n_b^\perp has polar coordinates $(r, \theta) = (1, 0)$.

Formulas (59) and (60) for the switching rate f_s have a 12-fold symmetry in β (f_s is unchanged by reflection in the axes of symmetry along $n_a^\perp, n_b^\perp, n_c^\perp, n_a, n_b, n_c$). Therefore, the average switching rate $\hat{f}_s(r)$ on a circle of radius r can be computed on a sector of the circle such as $\theta \in [0, \pi/6]$

$$\hat{f}_s(r) = \frac{6}{\pi} \int_0^{\pi/6} f_s(r, \theta) d\theta. \quad (62)$$

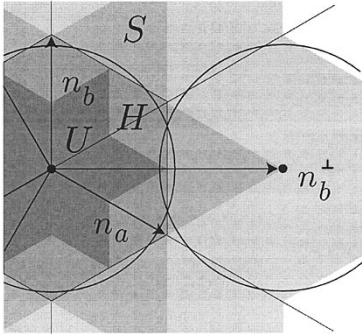
To evaluate (62), there are three cases according to how the sector of the circle intersects the regions U, H , and S .

Case A: $0 \leq r \leq \sqrt{3}/6$. The sector of the circle lies inside U and the switching rate formula (60) specializes to

$$f_s = \frac{4}{3} (\beta_b^\perp - \beta_a^\perp \beta_c^\perp) = \frac{8}{3} r \cos \theta + \frac{4}{3} r^2 (1 - 2 \cos 2\theta). \quad (63)$$

Evaluating (62) using (63) gives

$$\hat{f}_s = \frac{8}{\pi} r - \frac{4}{\pi} \left(\sqrt{3} - \frac{\pi}{3} \right) r^2, \quad 0 \leq r \leq \frac{\sqrt{3}}{6}. \quad (64)$$

Fig. 7. Sinusoidal input that lies partly outside H .

Case B: $\sqrt{3}/6 < r \leq 1/2$. The sector of the circle lies in U for $\theta \in [0, \theta_1]$ and in $H \cap U^c$ for $\theta \in (\theta_1, \pi/6]$. The boundary of U satisfies $|\beta_2^\perp| = |\beta_a^\perp| = 1/2$. Equations (27) and (61) yield

$$\theta_1 = \sec^{-1} \frac{8r}{1 + \sqrt{48r^2 - 3}}. \quad (65)$$

In $H \cap U^c$ switching rate formula (59) specializes to

$$\begin{aligned} f_s &= -\frac{1}{3} + \frac{4}{3} (\beta_b^\perp - \beta_a^\perp + \beta_b^\perp \beta_a^\perp) \\ &= -\frac{1}{3} + \frac{4}{3} r (3 \cos \theta + \sqrt{3} \sin \theta) \\ &\quad - \frac{8}{3} r^2 (\cos^2 \theta + \sqrt{3} \cos \theta \sin \theta). \end{aligned} \quad (66)$$

Evaluating (62) using (63) for $\theta \in [0, \theta_1]$ and (66) for $\theta \in (\theta_1, \pi/6]$ gives

$$\begin{aligned} \hat{f}_s &= \frac{2}{\pi} \theta_1 - \frac{1}{3} + \frac{16}{\pi} r \cos \left(\theta_1 + \frac{\pi}{6} \right) + \\ &4r^2 \left(\frac{4}{\pi} \theta_1 - \frac{1}{3} - \frac{2}{\pi} \cos \left(2\theta_1 - \frac{\pi}{6} \right) \right), \quad \frac{\sqrt{3}}{6} < r \leq \frac{1}{2}. \end{aligned} \quad (67)$$

Case C: $1/2 < r \leq 1/\sqrt{3}$. As shown in Fig. 7, the sector of the circle lies in $S \cap H^c$ for $\theta \in [0, \theta_2]$ and in $H \cap U^c$ for $\theta \in (\theta_2, \pi/6]$ where

$$\theta_2 = \sec^{-1} 2r. \quad (68)$$

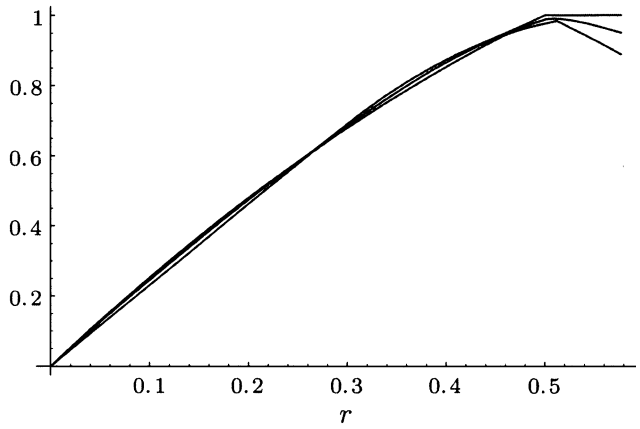
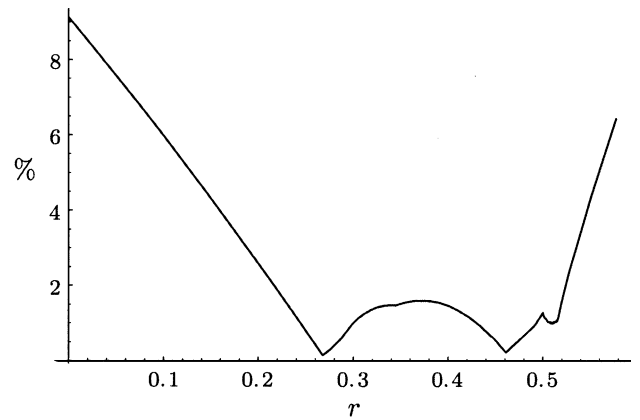
The switching rate for the sector of the circle in $S \cap H^c$ for $\theta \in [0, \theta_2]$ is equal to the switching rate for the reflection of this sector in the edge of the hexagon H . (The reflected sector may be obtained by mapping the sector inside H using \square and then reflecting in a vertical axis. According to (57) and the 12-fold symmetry of (60) and (59), these operations preserve the switching rate). The reflected sector is a sector of the circle of radius r centered on n_b^\perp and may be parameterized by $\theta \in [0, \theta_2]$ as $(1 - r \cos \theta, r \sin \theta)^t$ in rectangular coordinates and as

$$\begin{pmatrix} \beta_a^\perp \\ \beta_b^\perp \\ \beta_c^\perp \end{pmatrix} = \begin{bmatrix} -1 & \sqrt{3} \\ 2 & 0 \\ -1 & -\sqrt{3} \end{bmatrix} \begin{pmatrix} 1 - r \cos \theta \\ r \sin \theta \end{pmatrix} \quad (69)$$

in coordinates (21).

The reflected sector lies in U for $\theta \in [0, \theta_1]$ and in $H \cap U^c$ for $\theta \in (\theta_1, \theta_2]$. For $\theta \in [0, \theta_1]$, the switching rate is obtained using (63) and (69) as

$$f_s = \frac{4}{3} (1 + r^2 - 2r^2 \cos 2\theta). \quad (70)$$

Fig. 8. Minimum, maximum, and average switching rates for $0 \leq r < 1/\sqrt{3}$.Fig. 9. Normalized switching rate variation for $0 \leq r < 1/\sqrt{3}$.

For $\theta \in (\theta_1, \theta_2]$, the switching rate is obtained using (66) and (69) as

$$f_s = 1 + \frac{4}{3} r (2r \cos \theta - 1) (\sqrt{3} \sin \theta - \cos \theta). \quad (71)$$

Evaluating (62) using (70) for $\theta \in [0, \theta_1]$, using (71) for $\theta \in (\theta_1, \theta_2]$, and using (66) for $\theta \in (\theta_2, \pi/6]$ gives

$$\begin{aligned} \hat{f}_s &= -\frac{1}{3} + \frac{2}{\pi} \theta_1 + \frac{8}{\pi} \theta_2 - \frac{16}{\pi} r \\ &\quad \times \left(\cos \left(\theta_1 - \frac{\pi}{6} \right) - 2 \cos \left(\theta_2 + \frac{\pi}{6} \right) \right) \\ &\quad - \frac{4}{\pi} r^2 \left(\frac{\pi}{3} - 4\theta_1 - 2 \cos \left(2\theta_1 + \frac{\pi}{6} \right) + 2\sqrt{3} \cos 2\theta_2 \right), \\ &\quad \frac{1}{2} < r \leq \frac{1}{\sqrt{3}}. \end{aligned} \quad (72)$$

Formulas (64), (67), and (72) give the average switching rate \hat{f}_s over the range $0 \leq r \leq 1/\sqrt{3}$ and is plotted in Fig. 8. For $r = 1/2$ the average switching rate is 0.98732. Fig. 8 also plots the minimum and maximum switching rates.

Fig. 9 plots the variation of the switching rate against the radius of the sinusoidal input. The switching rate variation for a particular radius is defined as the maximum percentage the switching rate deviates from the average switching rate over the circle normalized to the average switching rate

$$\text{var} f_s(r) = \frac{100}{\hat{f}_s(r)} \max_{0 \leq \theta < 2\pi} |f_s(r, \theta) - \hat{f}_s(r)|. \quad (73)$$

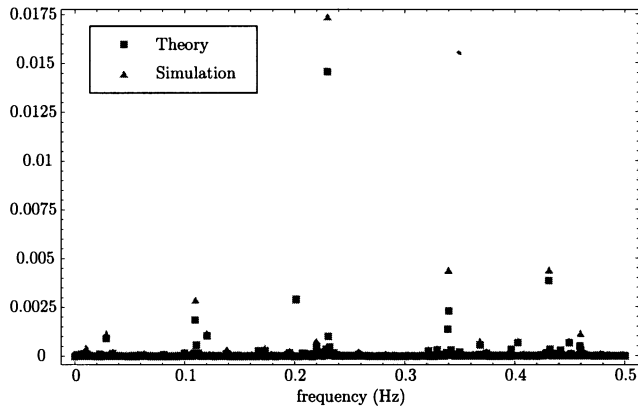


Fig. 10. Simulated and theoretical spectrum S_e of quantization error.

The maximum variation is 9% at zero radius. Note that the variation never reaches zero. This implies that the contours of Fig. 6 are never perfect circles. (Interestingly, the curve rises rapidly beyond $r = 1/2$, this is because in Fig. 8 the maximum switching rate is unity for $(1/2) \leq r < (1/\sqrt{3})$ while the minimum switching rate decreases fairly rapidly.)

VII. SIMULATION RESULTS

This section presents simulation results to illustrate and confirm the analytic results for the quantization error spectrum and average switching rate of the hexagonal $\Sigma\Delta$ modulator.

Numerical results for 1024 samples of the quantization error sequence e_n are obtained using recursion (32) for $\beta = (0.229\ 693, 0.339\ 432, -0.569\ 125)$ and $e_0 = 0$. Each component of β was chosen randomly with a precision of 30 digits to make it likely that the value of β was representative of the generic Case 1 within the limitations of finite precision computation.

The discrete Fourier transform of the error sequence is taken with a normalized frequency such that the sampling frequency equals one. The spectral density is evaluated at 1024 frequencies uniformly distributed in the range $[0,1)$ and is denoted by triangles in Fig. 10. Fig. 10 also shows the Bohr–Fourier spectrum predicted by formula (52) as boxes. The theoretical and simulated points correspond quite closely. Note that the discrete Fourier transform of the numerical results is computed at uniformly spaced frequencies whereas the Bohr–Fourier spectrum is computed for the frequencies $\langle p\beta \rangle$ with $p \in \Lambda^*$. The locations of the spikes correspond well, but their amplitudes differ somewhat. As expected, the error spectrum is neither continuous nor white. The quantization error sequence has mean 6.64×10^{-4} and variance 9.27×10^{-2} which agrees well with the theoretical results of Section V. The quantization error sequence mean and variance are close to that of a uniform sequence of random variables.

Fig. 11 shows the simulated average switching rate for sinusoidal inputs of amplitudes $0 \leq r < (1/\sqrt{3})$ compared to the average switching rate \hat{f}_s computed from formulas (64), (67), and (72). The simulation length is 65 536 points and the oversampling ratio is 64. The absolute maximum error between simulation and \hat{f}_s is 4.24×10^{-2} at $r = 0.128$ and the mean-squared error is 1.88×10^{-4} . The error can be reduced by increasing the

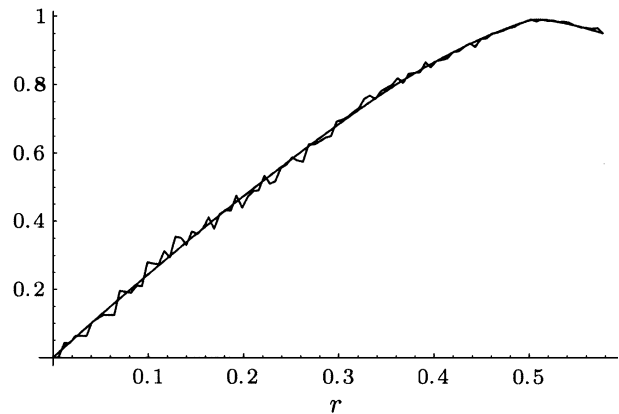


Fig. 11. Average switching rate simulation results and \hat{f}_s for $0 \leq r < 1/\sqrt{3}$.

oversampling ratio. For instance the mean-squared error reduces to 6.85×10^{-5} for an oversampling ratio of 256.

VIII. CONCLUSIONS

Switching states in power-electronic circuits may be thought of as determining quantized outputs which are passed through a lowpass filter to synthesize a given input signal. This process is analogous to quantizing, transmitting, and demodulating signals in communication systems. Pursuit of this analogy in the context of $\Sigma\Delta$ modulation with a natural choice of a nearest neighbor quantizer yields a hexagonal $\Sigma\Delta$ modulator for a voltage source inverter that is a nontrivial generalization of a scalar $\Sigma\Delta$ modulator.

The output spectrum and switching rate of the hexagonal $\Sigma\Delta$ modulator have complicated behavior and are key performance measures. We have applied ergodic theory and Fourier analysis to analytically compute the output spectrum and switching rate. We have found the interplay between the hexagonal geometry and the intricacies of the ergodic and harmonic analysis to be intriguing. These calculations are foundational for hexagonal $\Sigma\Delta$ modulators and for their application to power electronics.

APPENDIX I

FOURIER AND ERGODIC RESULTS ON H

We transform standard Fourier and ergodic results from the square $[0,1)^2$ to H . Relate coordinates x' on $[0,1)^2$ to coordinates x on H by $x' = \langle Vx \rangle$ and $x = \langle \overline{Wx'} \rangle$. Relate coordinates p on Λ^* to coordinates p' on \mathbb{Z}^{*2} by $p' = pW$. Suppose $f' \in L^2([0,1)^2)$ and let $f = f' \circ \langle \rangle \circ V \in L^2(H)$. Then $f'(x') = f'(\langle Vx \rangle) = f(x)$, $dx = |H|dx'$, and $\langle p'x' \rangle = \langle pW \langle Vx \rangle \rangle = \langle px \rangle$. Write $(f, g) = (1/|H|) \int_H f(x)g^*(x)dx$ and $(f', g') = \int_{[0,1)^2} f'(x')g'^*(x')dx'$. Then $(f, g) = (f', g')$ and $\hat{f}_p = (f, e^{-i2\pi px}) = (f', e^{-i2\pi p'x'}) = \hat{f}'_{p'}$. Moreover

$$\begin{aligned} f(\langle \overline{x+y} \rangle) &= f'(\langle V \langle \overline{x+y} \rangle \rangle) \\ &= f'(\langle V(x+y) \rangle) = f'(\langle x' + y' \rangle). \end{aligned}$$

Hence, the following results can be transformed to the results of Section III-D.

Fourier analysis on $[0,1)^2$ [41]: $L^2([0,1)^2)$ is a Hilbert space with inner product (f', g') . $\{e^{i2\pi p'x'} \mid p' \in \mathbb{Z}^{*2}\}$ is a complete orthonormal basis. $f'(x') = \sum_{p' \in \mathbb{Z}^{*2}} \hat{f}'_{p'} e^{i2\pi p'x'}$ where the

equality is interpreted in the L^2 sense and $\hat{f}'_{p'} = (f', e^{-i2\pi p'x'})$. The Parseval formula is $(f', g') = \sum_{p' \in \mathbb{Z}^{*2}} \hat{f}'_{p'} \hat{g}'_{p'}^*$.

Mané [40, Th.II 3.2, prop. II 2.7, Th. I 9.2] implies the following. Let $\beta' \in \mathbb{R}^2$ be such that the only $p' \in \mathbb{Z}^{*2}$ with $p'\beta' \in \mathbb{Z}$ is $p' = 0$. Let $\tilde{f}' : \mathbb{R}^2/\mathbb{Z}^2 \rightarrow \mathbb{R}$ be continuous. Let π be the canonical projection $\mathbb{R}^2 \rightarrow \mathbb{R}^2/\mathbb{Z}^2$. Then translation by $\pi\beta'$ is a uniquely ergodic shift on $\mathbb{R}^2/\mathbb{Z}^2$ and, for all $e'_0 \in \mathbb{R}^2$, $\lim_{L \rightarrow \infty} (1/L) \sum_{n=0}^{L-1} \tilde{f}'(\pi(e'_0 + n\beta')) = \int_{\mathbb{R}^2/\mathbb{Z}^2} \tilde{f}'(s') ds'$. (Note that $\pi(e'_0 + n\beta') = \pi \langle e'_0 + n\beta' \rangle$.) Suppose that $f' : [0, 1]^2 \rightarrow \mathbb{R}$ lifts to \tilde{f}' so that $f' = \tilde{f}' \circ \pi$. Then $\lim_{L \rightarrow \infty} (1/L) \sum_{n=0}^{L-1} f'(\langle e'_0 + n\beta' \rangle) = \int_{[0, 1]^2} f'(s') ds'$.

APPENDIX II THREE CASES FOR β

We characterize the three cases for $\beta \in H$.

Case 1 is $\{s \in \Lambda^* \mid s\beta \in \mathbb{Z}\} = \{0\}$. Suppose that Case 1 does not hold; that is, there is $r \in \Lambda^*$, $r \neq 0$ with $r\beta = z \in \mathbb{Z}$. We describe the general form of such a β . Suppose that $r = (r_1, r_2)V$ where $(r_1, r_2) \in \mathbb{Z}^{*2}$ and let g be the greatest common divisor of r_1, r_2 . By dividing r and z by any common factors of z and g , we may assume that z and g are relatively prime. Also, $r_1/g, r_2/g$ are relatively prime and by Euclid's algorithm there is $(\sigma_1, \sigma_2)^t \in \mathbb{Z}^2$ with $(r_1/g)\sigma_1 + (r_2/g)\sigma_2 = 1$. Let $\sigma = W(\sigma_1, \sigma_2)^t \in \Lambda$. Then, $r\sigma = g$ and $x = (z/g)\sigma$ is a particular solution to the equation $rx = z$. The general solution to $rx = z$ is $x = \alpha r_\perp + (z/g)\sigma$ where $r_\perp = W(-r_2, r_1)^t \in \Lambda$ and $\alpha \in \mathbb{R}$. Therefore

$$\beta = \alpha r_\perp + \frac{z}{g}\sigma \quad (74)$$

for some $\alpha \in \mathbb{R}$. Case 2 is α irrational and Case 3 is α rational.

First, we further characterize the β in Case 2 as satisfying

$$\{s \in \Lambda^* \mid s\beta \in \mathbb{Z}\} = \{mr \mid m \in \mathbb{Z}\} \quad (75)$$

$\{s \in \Lambda^* \mid s\beta \in \mathbb{Z}\} \supset \{mr \mid m \in \mathbb{Z}\}$ is clear. To prove $\{s \in \Lambda^* \mid s\beta \in \mathbb{Z}\} \subset \{mr \mid m \in \mathbb{Z}\}$, suppose that $s\beta = \alpha sr_\perp + (z/g)s\sigma = z' \in \mathbb{Z}$ for $s \in \Lambda^*$. Then, since $s\sigma \in \mathbb{Z}$, αsr_\perp must be rational, and it follows from α irrational that $0 = sr_\perp = (s_1, s_2)W \begin{pmatrix} -r_2 \\ r_1 \end{pmatrix} = r_1 s_2 - r_2 s_1$. Now

$$gs = \begin{pmatrix} s_1(r_1\sigma_1 + r_2\sigma_2) \\ s_2(r_1\sigma_1 + r_2\sigma_2) \end{pmatrix} = \begin{pmatrix} s_1 r_1 \sigma_1 + s_2 r_1 \sigma_2 \\ s_1 r_2 \sigma_1 + s_2 r_2 \sigma_2 \end{pmatrix} = s\sigma r \quad (76)$$

and $gz' = gs\beta = (s\sigma)r(z/g)\sigma = (s\sigma)z$. But g and z are relatively prime, so that g divides $s\sigma$ and (76) implies that $(s\sigma)/g = m$ is an integer such that $s = mr$.

Now we use (75) to prove in Case 2 that for $s \in \Lambda^*$

$$s\beta \in \mathbb{Z} \iff \left\{ \begin{array}{l} sr_\perp = 0 \\ s\sigma = 0 \pmod{g} \end{array} \right\}. \quad (77)$$

Suppose that $s\beta \in \mathbb{Z}$. Then, (75) implies that $s = mr$ for $m \in \mathbb{Z}$ and, hence, that $sr_\perp = 0$. Moreover, $s\beta = s((z/g)\sigma) = (z/g)s\sigma \in \mathbb{Z}$ and since g and z are relatively prime, g divides $s\sigma$ and $s\sigma = 0 \pmod{g}$. \Leftarrow in (77) follows from (74).

In Case 3, $\beta = \alpha r_\perp + (z/g)\sigma$ with α rational. Then, β has the form $\beta = (h/q)v$ for $v = W(v_1, v_2)^t \in \Lambda$, where h and q are integers. Without loss of generality we can assume that h and q are relatively prime and that v_1 and v_2 are relatively prime. By

Euclid's algorithm there is $(\rho_1, \rho_2) \in \mathbb{Z}^{*2}$ with $\rho_1 v_1 + \rho_2 v_2 = 1$. Let $\rho = (\rho_1, \rho_2)V \in \Lambda^*$. Also let $v_\perp = (-v_2, v_1)V \in \Lambda^*$.

We further characterize the β in Case 3 as satisfying $\{s \in \Lambda^* \mid s\beta \in \mathbb{Z}\} = \{z_1 v_\perp + z_2 q\rho \mid z_1, z_2 \in \mathbb{Z}\}$. It is clear that $\{s \in \Lambda^* \mid s\beta \in \mathbb{Z}\} \supset \{z_1 v_\perp + z_2 q\rho \mid z_1, z_2 \in \mathbb{Z}\}$. To prove $\{s \in \Lambda^* \mid s\beta \in \mathbb{Z}\} \subset \{z_1 v_\perp + z_2 q\rho \mid z_1, z_2 \in \mathbb{Z}\}$, suppose that $s\beta = (h/q)sv = z \in \mathbb{Z}$ with $s \in \Lambda^*$. Then, $hsv = qz$ and h and q relatively prime imply that h divides z and $z_2 = z/h$ is an integer. Then, $x = q(z/h)\rho = z_2 q\rho$ is a particular solution to the equation $x\beta = z$ with $x \in \Lambda^*$. The general solution to $x\beta = z$ is $x = z_1 v_\perp + z_2 q\rho$, $z_1 \in \mathbb{R}$. Since we require $x \in \Lambda^*$, $z_1 v_\perp = x - z_2 q\rho \in \Lambda^*$, and, since v_1 and v_2 are relatively prime, z_1 is an integer.

APPENDIX III FOURIER COEFFICIENTS FOR \square

We derive (39) for the Fourier coefficients of the hexagon part operator \square . Equation (38) implies $c_0 = 0$. Now, we compute c_p for $p \neq 0$. Define $a : \mathcal{P}^* \rightarrow \mathbb{R}$ by $a(p) = -\int_H e^{-i2\pi px} dx$. Then

$$c_p = \frac{1}{|H|} \int_H \square e^{-i2\pi ps} ds = \frac{1}{i2\pi |H|} (D_p a(p))^t \quad (78)$$

and the calculation reduces to finding

$$\begin{aligned} a(p) &= \frac{p}{i2\pi p p^t} \int_H (D_x e^{-i2\pi px})^t dx \\ &= \frac{p}{i2\pi |p|^2 |n_\perp^\perp|} \oint_{\partial H} e^{-i2\pi p \ell} n_\ell^\perp d\ell \\ &= \frac{|n|}{i2\pi |p|^2 |n_\perp^\perp|} \sum_{s \in \pm\{a, b, c\}} p n_s^\perp \int_{-1/2}^{1/2} e^{-i2\pi p \sigma_s(t)} dt \end{aligned}$$

where $\sigma_s(t) = (1/2)n_s^\perp + n_s t$, $t \in [-1/2, 1/2]$ parameterizes the hexagon edges. Letting $p_s = p n_s$ and $p_s^\perp = p n_s^\perp$ gives

$$\begin{aligned} a(p) &= \frac{-|n|}{\pi |n_\perp^\perp| |p|^2} \sum_{s \in \{a, b, c\}} p_s^\perp \int_{-1/2}^{1/2} \sin(2\pi p \sigma_s(t)) dt \\ &= \frac{-1}{\pi^2 \sqrt{3} |p|^2} \sum_{s \in \{a, b, c\}} \frac{p_s^\perp}{p_s} \sin(\pi p_s) \sin(\pi p_s^\perp). \quad (79) \end{aligned}$$

Substituting (79) in (78), differentiating, and evaluating at $p \in \Lambda^*$ (then $p_s^\perp \in \mathbb{Z}$ and $\sin(\pi p_s^\perp) = 0$) yields

$$c_p = \frac{i}{6\pi^2 |p|^2} \sum_{s \in \{a, b, c\}} \frac{p_s^\perp}{p_s} \sin(\pi p_s) \cos(\pi p_s^\perp) n_s^\perp. \quad (80)$$

When $p \in \Lambda^t - \{0\}$, $p_s \in \mathbb{Z}$ and $\sin(\pi p_s)/(\pi p_s) = 0$ and $c_p = 0$ except when $p_s = 0$. When $p_s = 0$, $p = k n_s^\perp$, $k \in \mathbb{Z}$, $p_s^\perp = 2k$ and (39) with $p \in \Lambda^t - \{0\}$ follows from (80).

To simplify (80) when $p \in \Lambda^* - \Lambda^t$, consider $f_s : \Lambda^* \rightarrow \mathbb{R}$

$$f_s(p) = 2 \sin(\pi p_s) \cos(\pi p_s^\perp) = \sin(\pi p n_s^+) + \sin(\pi p n_s^-)$$

where $n_s^\pm = n_s \pm n_s^\perp$. Note that $n_s^\pm \in 2\Lambda^{*t}$. Let $\lambda \in \Lambda$. Then $f_s(p + \lambda^t) = \sin(\pi(p + \lambda^t) n_s^+) + \sin(\pi(p + \lambda^t) n_s^-) = f_s(p)$ since $n_s^\pm \in 2\Lambda^{*t}$ implies that $\lambda^t n_s^\pm$ is an even integer. This periodicity of f_s implies that f_s is constant on each of $n_a^t + \Lambda^t$ and $-n_a^t + \Lambda^t$. The respective constants can be directly calculated

as $f_s(\pm n_a^t) = \pm\sqrt{3}$ for $s = a, b, c$. Then $f_s(p) = \text{sgn}(p)\sqrt{3}$ and, for $p \in \Lambda^* - \Lambda^t$

$$c_p = \frac{i \text{sgn}(p)}{4\sqrt{3}\pi^2|p|^2} \sum_{s \in \{a,b,c\}} \frac{p_s^\perp}{p_s} n_s^\perp$$

$$= \frac{i \text{sgn}(p)}{4\sqrt{3}\pi^2|p|^2} \begin{bmatrix} \frac{p_a - p_c}{p_b} + \frac{p_a - p_b}{p_c} \\ \frac{p_b - p_c}{p_a} + \frac{p_b - p_a}{p_c} \\ \frac{p_c - p_b}{p_a} + \frac{p_c - p_a}{p_b} \end{bmatrix}.$$

Using $p_a + p_b + p_c = 0$ we obtain (39) for $p \in \Lambda^* - \Lambda^t$.

APPENDIX IV ABSOLUTE SUMMABILITY

We prove that the coefficients $\sum_{p \in \Lambda^*} |[c_p \otimes c_p^*]_{i,j}| < \infty$.

For the case $p \in \{(n_a^t + \Lambda^t) \cup (-n_a^t + \Lambda^t)\}$, $c_p \sim p^t / \Pi(p)$.
Using $p = \pm n_a^t + (n_1, n_2)W^t$ where $(n_1, n_2) \in \mathbb{Z}^2$

$$\sum_{p \in \{(n_a^t + \Lambda^t) \cup (-n_a^t + \Lambda^t)\}} |[c_p \otimes c_p^*]_{i,j}| \sim \sum_{(n_1, n_2) \in \mathbb{Z}^2} \frac{1}{n_1^2 n_2^2} < \infty.$$

For the case $p \in \{\Lambda^t | p_a p_b p_c = 0, p \neq 0\}$, the sum is over points in three lines and $c_p \sim (p_a/p_b p_c, p_b/p_a p_c, p_c/p_a p_b)^t$.
Using $p = (n_1, n_2)W^t$ where $(n_1, n_2) \in \mathbb{Z}^2$

$$\sum_{p \in \{\Lambda^t | p_a p_b p_c = 0, p \neq 0\}} |[c_p \otimes c_p^*]_{i,j}| \sim \sum_{n \in \mathbb{Z}} \frac{1}{n^2} < \infty.$$

REFERENCES

- [1] J. C. Candy and G. C. Temes, Eds., *Oversampling Methods for A/D and D/A Conversion*. Piscataway, NJ: IEEE Press, 1992.
- [2] S. R. Norsworthy, R. Schreier, and G. C. Temes, Eds., *Delta-Sigma Data Converters: Theory, Design, and Simulation*. Piscataway, NJ: IEEE Press, 1997.
- [3] J. C. Candy and O. J. Benjamin, "The structure of quantization noise from sigma-delta modulation," *IEEE Trans. Commun.*, vol. COM-29, pp. 1316–1323, Sept. 1981.
- [4] J. C. Candy, "A use of double integration in sigma delta modulation," *IEEE Trans. Commun.*, vol. COM-33, no. 3, pp. 249–258, Mar. 1985.
- [5] G. Luckjiff, I. Dobson, and D. Divan, "Interpolative sigma-delta modulators for high frequency power-electronic applications," in *Proc. Power Electronics Specialists Conf.*, Atlanta, GA, June 1995, pp. 444–449.
- [6] T. G. Habetler and D. M. Divan, "Performance characterization of a new discrete pulse modulated current regulator," in *Proc. Ind. Appl. Soc.*, Pittsburgh, PA, Oct. 1988, pp. 395–405.
- [7] D. M. Divan, "The resonant dc link converter," in *Proc. Ind. Appl. Soc.*, Denver, CO, 1986, pp. 648–656.
- [8] H. Van Der Broeck, H. Skudelny, and G. Stanke, "Analysis and realization of a pulsewidth modulator based on voltage space vectors," *IEEE Trans. Ind. Appl.*, vol. 24, pp. 142–150, Feb. 1988.
- [9] J. H. Conway and N. J. A. Sloane, *Sphere Packings, Lattices and Groups*, 2nd ed. New York: Springer-Verlag, 1993.
- [10] A. Gersho, "On the structure of vector quantizers," *IEEE Trans. Inform. Theory*, vol. IT-28, pp. 157–166, Mar. 1982.
- [11] A. Gersho and R. M. Gray, *Vector Quantization and Signal Compression*. Boston, MA: Kluwer, 1992.
- [12] W. R. Bennett, "Spectra of quantized signals," *Bell Syst. Tech. J.*, vol. 27, pp. 446–472, 1948.
- [13] R. Schreier, "An empirical study of high order single bit delta sigma modulators," *IEEE Trans. Circuits Syst.*, vol. 40, pp. 461–466, Aug. 1993.
- [14] R. M. Gray, "Spectral analysis of quantization noise in a single-loop sigma-delta modulator with dc input," *IEEE Trans. Commun.*, vol. 37, pp. 588–599, June 1989.
- [15] —, "Oversampled sigma-delta modulation," *IEEE Trans. Commun.*, vol. COM-35, pp. 481–488, July 1987.
- [16] —, "Quantization noise spectra," *IEEE Trans. Inform. Theory*, vol. 36, pp. 1220–1244, Nov. 1990.
- [17] D. F. Delchamps, "Exact asymptotic statistics for sigma-delta quantization noise," in *Proc. Allerton Conf. Communication, Control, and Computing*, Urbana, IL, Oct. 1990, pp. 703–712.
- [18] —, "Spectral analysis of sigma-delta quantization noise," in *Proc. Information Sciences and Systems*, Baltimore, MD, Mar. 1990, pp. 167–172.
- [19] N. He, F. Kuhlmann, and A. Buzo, "Double-loop sigma-delta modulation with dc input," *IEEE Trans. Commun.*, vol. COM-38, pp. 106–114, Apr. 1990.
- [20] J. C. Kieffer, "Analysis of dc input response for a class of one-bit feedback encoders," *IEEE Trans. Commun.*, vol. COM-38, pp. 337–340, Mar. 1990.
- [21] S. Hein and A. Zakhov, "On the stability of sigma-delta modulators," *IEEE Trans. Signal Processing*, vol. 41, pp. 2322–2348, July 1993.
- [22] H. Wang, " $\Sigma\Delta$ modulation from the perspective of nonlinear dynamics," in *Proc. ISCAS'92*, vol. 3, May 1992, pp. 1296–1299.
- [23] O. Feely, D. Fournier-Prunaret, I. Taralova-Roux, and D. Fitzgerald, "Nonlinear dynamics of bandpass sigma-delta modulation – An investigation by means of the critical lines tool," *Int. J. Bifurcations Chaos*, vol. 10, no. 2, pp. 307–323, 2000.
- [24] G. Luckjiff and I. Dobson, "Power spectrum of a sigma-delta modulator with hexagonal vector quantization and constant input," in *Proc. Int. Symp. Circuits and Systems*, vol. 5, Orlando, FL, May 1999, pp. 270–273.
- [25] A. Boehringer and F. Brugger, "Transformatorlose transistor-pulsrichter mit ausgangsleistungen bis 50 kva," *Elektr. Masch.*, vol. 96, no. 12, pp. 538–545, 1979.
- [26] B. Schwarz, "Beiträge zu Reaktionsschnellen und Hochge Nauen Drehstrom-Positionier-Systemen," Ph.D. dissertation, Univ. Stuttgart, Stuttgart, Germany, 1986.
- [27] M. Kheraluwala and D. M. Divan, "Delta modulation strategies for resonant link inverters," in *Proc. Power Electronics Specialists Conf.*, Blacksburg, VA, June 1987, pp. 271–278.
- [28] D. R. Seidl, "Motion and Motor Control Using Structured Neural Networks," Ph.D. dissertation, Dep. Elect. Comp. Eng., University of Wisconsin-Madison, Madison, WI, 1996.
- [29] G. Venkataraman, D. M. Divan, and T. M. Jahns, "Discrete pulse modulation strategies for high-frequency inverter systems," in *Proc. Power Electronics Specialists Conf.*, vol. 2, Milwaukee, WI, June 1989, pp. 1013–1020.
- [30] A. Mertens, "Performance analysis of three-phase inverters controlled by synchronous delta-modulation systems," *IEEE Trans. Ind. Appl.*, vol. 30, pp. 1016–1027, Aug. 1994.
- [31] J. P. Vilain and C. Lesbroussart, "A new space vector modulation strategy for a three-phase inverter: The space vector based delta-sigma modulation," *J. Phys. III*, vol. 5, no. 7, pp. 1075–1088, 1995.
- [32] G. Venkataraman, "Topology, Analysis and Control of a Resonant dc Link Power Converter," Ph.D. dissertation, Dep. Elect. Comp. Eng., University of Wisconsin-Madison, Madison, WI, 1992.
- [33] A. Mertens and H. Skudelny, "Calculations on the spectral performance of discrete pulse modulation strategies," in *Proc. Power Electronics Specialists Conf.*, Boston, MA, June 1991, pp. 357–365.
- [34] J. Nieźnanski, "Performance characterization of vector sigma-delta modulation," in *Proc. Ind. Elect. Soc. Conf.*, vol. 1, Aachen, Germany, Aug–Sept. 1998, pp. 531–536.
- [35] G. Luckjiff, I. Dobson, and D. M. Divan, "Modulator for Resonant Link Converters," U.S. Patent no. 5 619 406, Apr. 8 1997.
- [36] H. Furstenberg, *Recurrence in Ergodic Theory and Combinatorial Number Theory*. Princeton, NJ: Princeton Univ. Press, 1981.
- [37] C. Corduneanu, *Almost Periodic Functions*. New York: Wiley, 1968.
- [38] Y. Katznelson, *An Introduction to Harmonic Analysis*, 2nd ed. New York: Dover, 1976.
- [39] W. Rudin, *Fourier Analysis on Groups*. New York: Wiley, 1962.
- [40] R. Mäné, *Ergodic Theory and Differentiable Dynamics*. New York: Springer-Verlag, 1987.
- [41] A. Zygmund, *Trigonometric Series*, 2nd ed. Cambridge, U.K.: Cambridge Univ. Press, 1959.



Glen Luckjiff received the B.S., M.S., and Ph.D. degrees from the Lafayette College, Easton, PA, the Rensselaer Polytechnic Institute, Troy, NY, and the University of Wisconsin, Madison, in 1989, 1991, and 2002, respectively, in electrical engineering, and the M.S. degree in financial mathematics from the University of Chicago, Chicago, IL, in 2003.

In 1991, he was with GE Corporate Research and Development, Schenectady, NY, and since 1995, has been with Soft Switching Technologies Corporation, Madison, WI. His research interests include sigma-delta modulation and the control of power-electronic systems.



Ian Dobson (M'89–SM'98) received the B.A. degree in math from Cambridge University, Cambridge, U.K., in 1978, and the Ph.D. degree in electrical engineering from Cornell University, Ithaca, NY, 1989.

He was a Systems Analyst for EASAMS Ltd, Frimley, U.K., from 1978 to 1983. In 1989, he joined the University of Wisconsin-Madison, where he is now a Professor in Electrical and Computer Engineering. His current interests are applications of complex systems, nonlinear dynamics, electric power system instabilities, power electronics, and

self-organized criticality.